Annals of Nuclear Energy 173 (2022) 109105

Contents lists available at ScienceDirect

Annals of Nuclear Energy

journal homepage: www.elsevier.com/locate/anucene

Effect of fuel nuclide composition on the fuel lifetime of the RITM-200 reactor unit

S. Beliavskii *, N. Anikin, S. Alhassan, S. Kudeev, V. Nesterov

Division for Nuclear-Fuel Cycle, School of Nuclear Science and Engineering, National Research Tomsk Polytechnic University, 634050, Lenina ave 30, Tomsk, Russia

ARTICLE INFO

Article history:
Received 27 January 2022
Received in revised form 21 March 2022
Accepted 26 March 2022
Available online 1 April 2022

Keywords:
RITM-200 reactor
Effective multiplication factor
Pressurized water reactor
Thorium-uranium fuel cycle
Uranium–plutonium fuel cycle
Multigroup calculation
Small modular reactor

ABSTRACT

This paper describes the methodology used in determining the fuel lifetime of the RITM-200, a small modular 200 MWth pressurized water reactor (PWR), under operating conditions. Three different dispersed fuel compositions, namely (^{238}U + ^{235}U)O_2, (^{232}Th + ^{235}U)O_2, and (^{232}Th + ^{233}U)O_2, were examined for the calculation of the fuel lifetime. Switching the fuel composition from (^{238}U + ^{235}U)O_2 to (^{232}Th + ^{233}U)O_2 extends the fuel lifetime by 44% and the fuel burnup by 60% at the design values of the fuel element diameter. The dependency of the fuel lifetime and fuel burnup on the diameter was also determined. This study shows that the most efficient fuel composition is (^{232}Th + ^{233}U)O_2 with the fuel diameter increased to 7.9 mm as it extends the fuel lifetime of RITM-200 by 78% and its burnup by 50% compared to the design values of the fuel diameter.

1. Introduction

At the IAEA International Conference on Climate Change and the Role of Nuclear Power held in October 2019, the participated Member states expressed an opinion that small modular reactors might become the most efficient carbon-free energy option to replace obsolete fossil-fueled power plants (IAEA, 2020).

There are more than 50 projects of small modular reactors at the moment (IAEA, 2020). These types of reactors can satisfy the need in providing flexible power production, possessing enhanced passive safety systems and the capability of operating in heat supply as well as water desalination modes even in combination with alternative energy sources (IAEA, 2018).

The decentralized power supply is becoming more topical nowadays as there is a huge development of remote regions, perceived growth in the economy of developing countries, and the increasing demand for desalinated water. Small modular reactors are capable of fulfilling these purposes (Krushelnitskii, 2015; Bedenko et al., 2019; Shamanin et al., 2015; Hernandez and Brown, 2020; Karimi et al., 2021).

The northern regions of the Russian Federation have serious power supply issues due to the heavy reliance on obsolete low-power diesel generators and coal power plants. This situation has resulted in an increase in power rates by 5 to 55 times (from 22 to 237 rubles per kWh) compared to average power rates of 3 to 4 rubles per kWh in areas with centralized power supply in the country (Melnikov et al., 2020; Zmieva, 2020; Bashmakov, 2017; Lebedev and Shadrin, 2011).

The introduction of small modular reactors with maximal nuclear fuel lifetime would improve the economic efficiency and competitiveness of the power supply in these regions.

The idea of fuel lifetime extension is being widely discussed in research papers. In (Braslavskiy et al., 2019) authors state that extension of fuel lifetime for VVER-1000 from 480 to 1000 effective days would increase cost of produced power by 10%.

The extension of fuel lifetime can be achieved by using thorium in nuclear fuel. Thorium in pressurized water reactors is discussed in (Galahom et al., 2022), where the authors declare that a (^{232}Th, ^{233}U)O_2 fuel is capable of increasing the fuel lifetime and decreasing of actinide inventory at the end of the fuel cycle. Similar results for actinide inventory have been achieved by authors of (Rose et al., 2011).

The use of thorium-based fuel in small modular reactors is discussed in (Uguru et al., 2020), where the authors state that the use of thorium leads to a decrease in plutonium inventory at the end of the cycle. Besides, they state that thorium-based fuels can be used to achieve higher burnup. In addition to that, the authors of (Beliavskii et al., 2020) showed that thorium-uranium fuel

* Corresponding author.
E-mail address: svb28@tpu.ru (S. Beliavskii).

https://doi.org/10.1016/j.anucene.2022.109105
0306-4549/

composition can increase fuel lifetime by 42% in comparison to the standard fuel composition.

Low power nuclear power plant is a nuclear power plant equipped with two enhanced integral reactor units of RITM-200 (“Reactor Integralnii Transportnii Morskoi” or Integral Marine Transport Reactor of 200 MWth (PWR)) with a prior application in nuclear icebreakers (Petrunin et al., 2019).

The integral design of RITM-200 enhances the reactor pressure vessel manufacturability, cuts its production costs and time as the main equipment is placed inside the vessel of the steam generating unit.

Icebreaker reactors are mobile, resistant to external influences, possess self-protecting properties and capable of operating in maneuver mode while checking absorbed power.

The RITM-200 reactor core comprises fuel assemblies, safety rods, start-up neutron sources, and guide sleeves. Fuel rods contain dispersed fuel at the enrichment of 19 wt% of ^{235}U that meets the conditions of non-proliferation (Petrunin et al., 2019; Kostin et al., 2004).

This paper aims at determining the influence of fuel nuclide composition, the dependency of fuel element diameter on the fuel lifetime and the burnup of the RITM-200 reactor unit. An increase in these parameters would increase the competitiveness of RITM-200.

2. Design features of the RITM-200 reactor unit

The RITM-200 reactor core consists of 199 fuel assemblies (FA) (Fig. 1). The fuel assembly comprises 72 fuel elements, a central displacer with an absorbing shim rod, and 12 burnable poison rods (BPR). Each FA is placed inside a hexagonal canister with the width across flats of 98.5 mm and canister wall thickness of 1.65 mm. The hexagonal canisters are made of E-110 alloy. BPRs and fuel elements are situated at the regular triangular grid points with a pitch of 9.95 mm. The fuel element cladding, which is 1650 mm high and 6.9 mm in diameter, is made of 42CrNM alloy. Fuel comprises uranium dioxide particles dispersed inside a matrix made of silumin. Silumin is an aluminium alloy with 10 wt% of silicon. Not only does the silumin matrix contain fuel particles, but also it conducts heat and allows decreasing the maximum temperature of the fuel. Each fuel element contains 41.13 g of ^{235}U at a fuel enrichment of 19 wt %. The central hexagonal displacer of 31 mm width across flats and with 0.7 mm wall thickness is made of 42CrNM alloy. BPRs of 6.9 mm in diameter are placed at the periphery of the FA and BPRs of 4.5 mm in diameter are placed around the central displacer. BPRs are made of boron carbide. A cylindrical control rod, which is made of boron carbide, of 23 mm in diameter and with 2.5 mm wall thickness is placed in the center of the FA (Petrunin et al., 2019; Samoilov et al., 2017; Zakharychev et al., 2019).

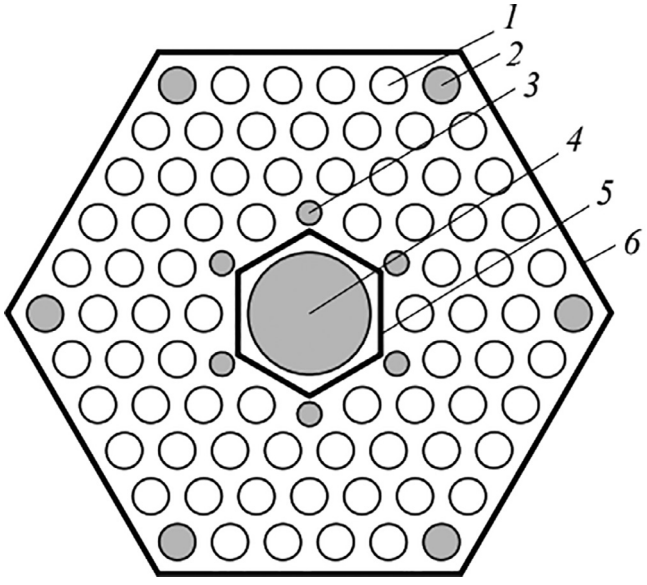

Fig. 1. Calculation model of RITM-200 fuel assembly: 1 - fuel rod; 2 - burnable poison rod with the 6.9-mm diameter; 3 - burnable poison rod with the 4.5-mm diameter; 4 - control rod; 5 - central hexagonal displacer; 6 - hexagonal canister.

In this study, the reactor core is composed of equivalent cells with the same nuclide content, sizes, and water-fuel ratio. Table 1 contains the data used for calculations.

3. Methods of the reactivity margin and fuel burnup calculation

The neutron flux spectrum was calculated through the following iteration algorithm of with the use of a set of multigroup diffusion equations for a critical nuclear reactor (stationary problem) (Kosheev et al., 2014; Golovatskiy et al., 2010):

$$D^{(i)} \cdot \Delta\Phi^{(i)} - \Sigma_a^{(i)} \cdot \Phi^{(i)} - \sum_{k=i+1}^{I} \Sigma_R^{i\to k} \cdot \Phi^{(i)} + \sum_{k=1}^{i-1} \Sigma_R^{k\to i} \cdot \Phi^{(k)} + \\ + \varepsilon^{(i)} \cdot \sum_{k=1}^{I} \nu_f^{(k)} \cdot \Sigma_f^{(k)} \cdot \Phi^{(k)} = 0, \quad (1)$$

where i signifies the counting number of the neutron group (the total amount of groups I is 26); k refers to the amount of the neutron groups; D_i denotes the diffusion coefficient for the i-th group of neutrons (cm^{-1}); Φ_i and Φ_k show the neutron flux in the k-th and i-th groups ($cm^{-2}\cdot s^{-1}$), respectively; $\Sigma_a^{(i)}$ represents the macroscopic cross-section of absorption for the i-th group of neutrons (cm^{-1}); $\Sigma_R^{i\to k}$, $\Sigma_R^{k\to i}$ signifies the macroscopic cross-sections of neutron removal from the i-th group to the k-th group and from the k-th group to the i-th group (cm^{-1}), respectively; $\varepsilon^{(i)}$ denotes the probability that a neutron will be in the i-th group immediately after fission; $\nu_f^{(k)}$ indicates the average number of neutrons per fission act in the i-th group of neutrons; $\Sigma_f^{(k)}$ represents the macroscopic cross-section of fission for the i-th group of neutrons (cm^{-1}).

The neutron flux value in the i-th group at j-th iteration was determined as follows:

Table 1
The main design features of the RITM-200 reactor core.

Parameter	Value
Core height (H_c), mm	1650
Core outer diameter (D_c), mm	1566
Fuel assemblies pitch, mm	101
Amount of FA in the reactor core	199
Volume of the reactor core, m^3	2.9
Amount of thermal energy produced per fuel lifetime, TW*h	7
Service life limit, h	48,500
Type of fuel elements	Plain-type cylindrical in 42CrNM alloy cladding
Fuel composition	UO_2 + silumine
Enrichment, wt%	19
Diameter of a fuel element and a burning poison rod, mm:	
Outer	6.9
Inner	6.3
Fuel element pitch in a fuel assembly, mm	9.95
BPR cladding material	42CrNM alloy
Width across sides of a fuel assembly hexagonal canister, mm	98.5
Thickness of a hexagonal canister, mm	1.65
Material of a hexagonal canister	E-110 alloy

$$\Phi_j^{(i)} = \frac{\varepsilon^{(i)} \cdot \sum_{\substack{k=1 \\ k\neq i}}^{26} \nu_f^{(k)} \cdot \Sigma_f^{(k)} \cdot \Phi_{j-1}^{(k)} + \sum_{k=1}^{i-1} \Sigma_R^{k\to i} \cdot \Phi_j^{(k)}}{D^{(i)} \cdot B_{(i)}^2 + \Sigma_a^{(i)} + \sum_{k=i+1}^{26} \Sigma_R^{i\to k} - \varepsilon^{(i)} \cdot \nu_f^{(i)} \cdot \Sigma_f^{(i)}}. \quad (2)$$

At the initial iteration, the number of neutrons produced in the second generation during the fission events induced by the first-generation neutrons was equal to 1:

$$\sum_{k=1}^{26} \nu_f^{(k)} \cdot \Sigma_f^{(k)} \cdot \Phi^{(k)} = 1 \quad (3)$$

The neutron flux value in the i-th group at the 0-th iteration.

$$\Phi_0^{(i)} = \frac{\varepsilon^{(i)} + \sum_{k=1}^{i-1} \Sigma_R^{k\to i} \cdot \Phi_0^{(k)}}{D^{(i)} \cdot B_{(i)}^2 + \Sigma_a^{(i)} + \sum_{k=i+1}^{26} \Sigma_R^{i\to k}}. \quad (4)$$

The total neutron flux was calculated as follows:

$$\Phi_\Sigma = \frac{Q_{th}}{\overline{\Sigma_f} \cdot E_f \cdot V_c}, \quad (5)$$

where Q_{th} denotes thermal power of the nuclear reactor (W); $\overline{\Sigma_f}$ denotes the average macroscopic cross-section of fission (cm^{-1}); E_f denotes the energy produced during the fission of a uranium nucleus, (J); V_c signifies the reactor core volume, (cm^3).

Microscopic cross-sections were taken from the ABBN evaluated neutron cross-section data (Kosheev et al., 2014). Calculations considered the Bondarenko f-factors of the resonance self-shielding as well as adjustment factors of the neutron gas temperature for the thermal group.

The resonance self-shielding was taken into account by means of the next formula:

$$\sigma_n = \sigma_{n0} \cdot f_n, \quad (6)$$

where σ_n refers to the microscopic cross-section of the n-th process with resonance self-shielding considered (barn); σ_{n0} denotes the microscopic cross-section of the n-th process without self-shielding process (barn); f_n signifies the Bondarenko f-factors of the resonance self-shielding.

To consider adjustment factors for thermal group (Kosheev et al., 2014; Bartolomey et al., 2012; Ganev, 1992), the following formula was used:

$$\sigma_m = \sigma_{m0} \cdot \frac{\sqrt{\pi}}{2} \cdot \sqrt{\frac{293}{T_{n.g.}}}, \quad (7)$$

where σ_m denotes the microscopic cross-section of m-th process with the neutron gas temperature considered (barn); σ_{m0} signifies the microscopic cross-section of m-th process without the effect of neutron gas temperature (barns).

To calculate the neutron gas temperature, the following formula was used:

$$T_{n.g.} = \frac{T_{in} + T_{out}}{2} \cdot \left(1 + 1{,}4 \cdot \frac{\Sigma_a(H_2O)}{\xi(H_2O) \cdot \Sigma_s(H_2O)}\right), \quad (8)$$

where T_{in} and T_{out} show the water temperature at the inlet and outlet of reactor core, respectively (K); $\Sigma_a(H_2O)$ refers to the macroscopic cross-section of absorption of the coolant (cm^{-1}); $\Sigma_s(H_2O)$ denotes the macroscopic cross-section of scattering of the coolant (cm^{-1}); $\xi(H_2O)$ signifies the moderation ability of the coolant.

The calculations of the effective multiplication factor were carried out by means of the next formula:

$$k_{eff} = \frac{\overline{\nu_f \cdot \Sigma_f}}{\overline{D \cdot B^2} + \overline{\Sigma_a}}, \quad (9)$$

where $\bar{\nu}_f$ indicates the average amount of neutrons per fission act; $\overline{\Sigma_f}$ denotes the average macroscopic cross-section of fission (cm^{-1}); $\overline{D}$ signifies the average diffusion coefficient (cm); $\overline{B^2}$ refers to the average buckling (cm^{-2}); $\overline{\Sigma_a}$ denotes the average macroscopic cross-section of absorption (cm^{-1}).

$$\overline{\nu_f \cdot \Sigma_f} = \sum_{i=1}^{I} \nu_f^{(i)} \cdot \Sigma_f^{(i)} \cdot \delta^{(i)}, \quad (10)$$

where $\nu_f^{(i)}$ indicates the average number of neutrons per fission act in the i-th group of neutrons; $\Sigma_f^{(i)}$ denotes the average macroscopic cross-section of fission (cm^{-1}); $\delta^{(i)}$ shows the partial neutron flux:

$$\delta^{(i)} = \frac{\Phi_i}{\sum_{i=1}^{I} \Phi_i}. \quad (11)$$

$$\overline{\Sigma_a} = \sum_{i=1}^{I} \Sigma_a^{(i)} \cdot \delta^{(i)}, \quad (12)$$

where $\Sigma_a^{(i)}$ represents the macroscopic cross-section of absorption for the i-th group of neutrons (cm^{-1});

$$\overline{D \cdot B^2} = \sum_{i=1}^{I} D^{(i)} \cdot B_{(i)}^2 \cdot \delta^{(i)}, \quad (13)$$

where $D^{(i)}$ denotes diffusion coefficient for the i-th group of neutrons (cm); $B_{(i)}^2$ refers to buckling for the i-th group of neutrons (cm^{-2}).

The fuel lifetime calculation takes into account the burnup of uranium and plutonium nuclei and the influence of ^{235}U and ^{238}U fission products.

To calculate fuel nuclide content for the uranium nuclear fuel cycle, the following equations were used:

$$\begin{aligned}
N_{i+1}^{235\,U} &= N_i^{235\,U} \cdot (1 - \overline{\sigma_a^{235\,U}} \Phi_\Sigma \cdot \Delta t);\\
N_{i+1}^{238\,U} &= N_i^{238\,U} \cdot (1 - \overline{\sigma_a^{238\,U}} \cdot \Phi_\Sigma \cdot \Delta t);\\
N_{i+1}^{239\,Pu} &= N_i^{239\,Pu} + (\overline{\sigma_c^{238\,U}} \cdot N_i^{238\,U} - \overline{\sigma_a^{239\,Pu}} \cdot N_i^{239\,Pu}) \cdot \Phi_\Sigma \cdot \Delta t;\\
N_{i+1}^{240\,Pu} &= N_i^{240\,Pu} + (\overline{\sigma_c^{239\,Pu}} \cdot N_i^{239\,Pu} - \overline{\sigma_a^{240\,Pu}} \cdot N_i^{240\,Pu}) \cdot \Phi_\Sigma \cdot \Delta t;\\
N_{i+1}^{241\,Pu} &= N_i^{241\,Pu} + (\overline{\sigma_c^{240\,Pu}} \cdot N_i^{240\,Pu} - \overline{\sigma_a^{241\,Pu}} \cdot N_i^{241\,Pu}) \cdot \Phi_\Sigma \cdot \Delta t;\\
N_{i+1}^{242\,Pu} &= N_i^{242\,Pu} + (\overline{\sigma_c^{241\,Pu}} \cdot N_i^{241\,Pu} - \overline{\sigma_a^{242\,Pu}} \cdot N_i^{242\,Pu}) \cdot \Phi_\Sigma \cdot \Delta t;\\
N_{i+1}^{FP235\,U} &= N_i^{FP235\,U} + 2 \cdot \overline{\sigma_f^{235\,U}} \cdot N_i^{235\,U} \cdot \Phi_\Sigma \cdot \Delta t;\\
N_{i+1}^{FP239\,Pu} &= N_i^{FP239\,Pu} + 2 \cdot \overline{\sigma_f^{239\,Pu}} \cdot N_i^{239\,Pu} \cdot \Phi_\Sigma \cdot \Delta t,
\end{aligned} \quad (14)$$

where N_i^j and N_{i+1}^j signify the initial and final concentrations of the corresponding nuclide (cm^{-3}), respectively; $\overline{\sigma_k}$ denotes the averaged by spectrum macroscopic cross-section for k-th reaction (barn).

$$\overline{\sigma_k} = \sum_{i=1}^{I} \sigma_{ki} \cdot \delta_i; \quad (15)$$

where Φ_Σ indicates the total neutron flux density along the neutron spectrum ($cm^{-2} \cdot s^{-1}$); Δt represents the step of temporal integration (s).

To determine fuel nuclide content for the thorium-uranium nuclear fuel cycle, the following equations were used:

$$
\begin{aligned}
N_{i+1}^{233\ U} &= N_i^{233\ U} + (\overline{\sigma_c^{232\ Th}} \cdot N_i^{232\ Th} - \overline{\sigma_a^{233\ U}} \cdot N_i^{233\ U}) \cdot \Phi_\Sigma \cdot \Delta t;\\
N_{i+1}^{234\ U} &= N_i^{234\ U} + (\overline{\sigma_c^{233\ U}} \cdot N_i^{233\ U} - \overline{\sigma_a^{234\ U}} \cdot N_i^{234\ U}) \cdot \Phi_\Sigma \cdot \Delta t;\\
N_{i+1}^{235\ U} &= N_i^{235\ U} + (\overline{\sigma_c^{234\ U}} \cdot N_i^{234\ U} - \overline{\sigma_a^{235\ U}} \cdot N_i^{235\ U}) \cdot \Phi_\Sigma \cdot \Delta t;\\
N_{i+1}^{232\ Th} &= N_i^{232\ Th} \cdot (1 - \overline{\sigma_a^{232\ Th}} \cdot \Phi_\Sigma \cdot \Delta t);\\
N_{i+1}^{FP233\ U} &= N_i^{FP233\ U} + 2 \cdot \overline{\sigma_f^{233\ U}} \cdot N_i^{233\ U} \cdot \Phi_\Sigma \cdot \Delta t;\\
N_{i+1}^{FP235\ U} &= N_i^{FP235\ U} + 2 \cdot \overline{\sigma_f^{235\ U}} \cdot N_i^{235\ U} \cdot \Phi_\Sigma \cdot \Delta t.
\end{aligned}
\tag{16}
$$

The effect of xenon and samarium poisoning on neutron flux and nuclide composition was omitted.

Fuel burnup values were determined by means of the following equation (Ganev, 1992):

$$B = \frac{Q_{th} \cdot t}{m_f}, \tag{17}$$

where Q_{th} denotes thermal power of nuclear reactor (MWth); t indicates the nuclear fuel lifetime (eff. days); m_f represents the mass of nuclear fuel (kg).

4. Effect of fuel nuclide composition on the fuel lifetime

The (^{238}U + ^{235}U)O_2, (^{232}Th + ^{235}U)O_2, and (^{232}Th + ^{233}U)O_2 dispersed fuel compositions were considered. The enrichment in all three variants was assumed to be 19 wt%. The fuel-matrix ratio in all compositions is the same: 43.5% of fuel and 56.5% of silumin matrix. The time step was assumed to be of 50 effective days. At every step, values of effective multiplication factor and reactivity margin were determined without excessive reactivity compensation by means of neutron absorbers (e.g., boric acid or boron carbide control rods). Afterwards, the value of the homogenized boron carbide concentration was determined in a way that the effective multiplication factor would be approximately equal to 1.

Table 2 shows the calculation results of the values of the effective multiplication factor (k_{eff}), the infinite multiplication factor (k_∞), the reactivity margin (ρ), the fuel lifetime, and the burnup (B) for the dispersed fuel compositions mentioned above. Table 3 contains the values of the fissile utilization in comparison to VVER-1000.

Table 2
Reactivity margin, fuel lifetime, and fuel burnup in the RITM-200 reactor unit for different dispersed fuel compositions.

Fuel composition	Reactivity margin	Fuel lifetime, eff. days	B, MW·d/kg_U
(^{238}U + ^{235}U)O_2	0.2351	1350	76.16
(^{232}Th + ^{235}U)O_2	0.2167	1400	87.37
(^{232}Th + ^{233}U)O_2	0.3270	1950	121.75

Table 3
Fissile utilization for the fuel types and comparison to VVER fuel.

Reactor and fuel type	VVER (UO2)	RITM-200 (^{238}U+^{235}U)	RITM-200 (^{232}Th+^{235}U)	RITM-200 (^{232}Th+^{233}U)
Enrichment, kg_{fiss}/kg_{HM}	0.045	0.19	0.19	0.19
Burnup, MWth·d/kg	53	76	87	122
Fissile utilization MWth·d/kg_{fiss}	1187	401	460	641

Fig. 2 illustrates the dependence of reactivity margin on the reactor operation time. Figs. 3 and 4 depict the dependences of the effective multiplication factor on the reactor operation time and on the burnup. Figs. 5 and 6 show the dependences of the infinite multiplication factor on the reactor operation time and on the burnup. Figs. 7 and 8 illustrate the dependences of the core leakage reactivity (difference between k_∞ and k_{eff}) on the reactor operation time and fuel burnup.

The obtained results show that the switch from (^{238}U + ^{235}U)O_2 to (^{232}Th + ^{235}U)O_2 results in an increase in the fuel lifetime by 3.7% and the burnup by 14.7%. The switch from (^{238}U + ^{235}U)O_2 to (^{232}Th + ^{233}U)O_2 results in an increase of the fuel lifetime by 44.4% and the burnup by 59.9%. This happens due to ^{233}U having higher fission efficiency than ^{235}U. Moreover, ^{233}U is produced due to the

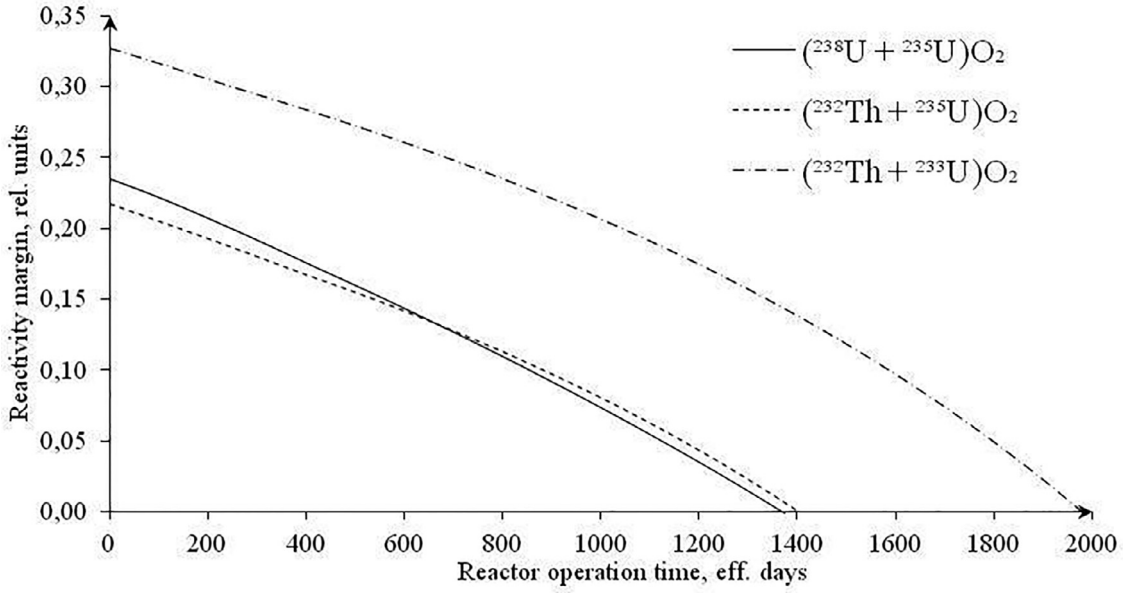

Fig. 2. Reactivity margin evolution with the reactor operation time for different dispersed nuclear fuel.

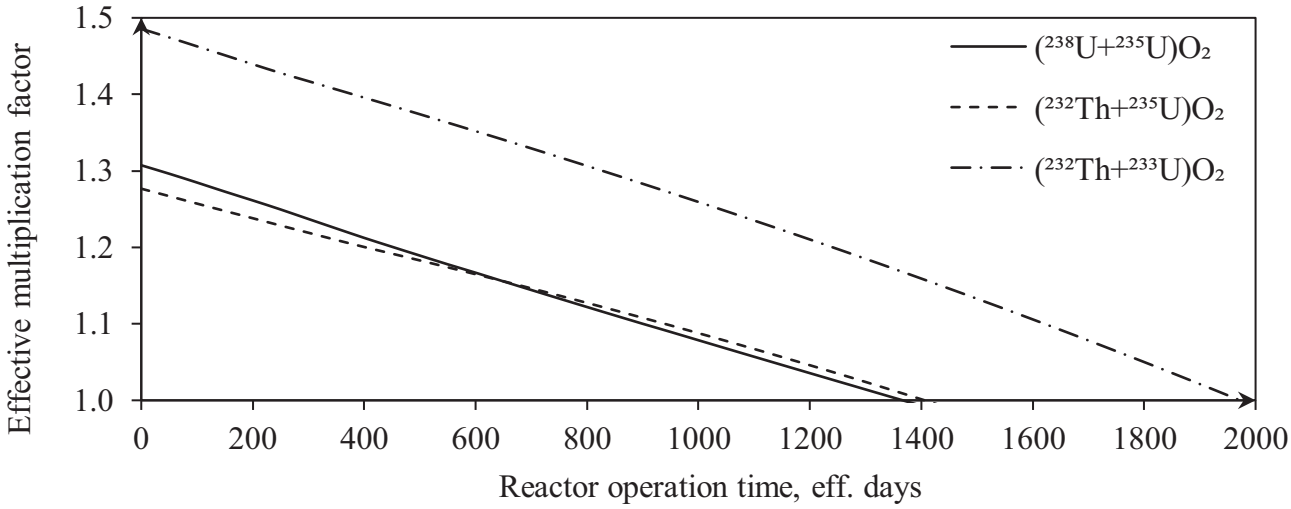

Fig. 3. The dependence of the effective multiplication factor on the reactor operation time.

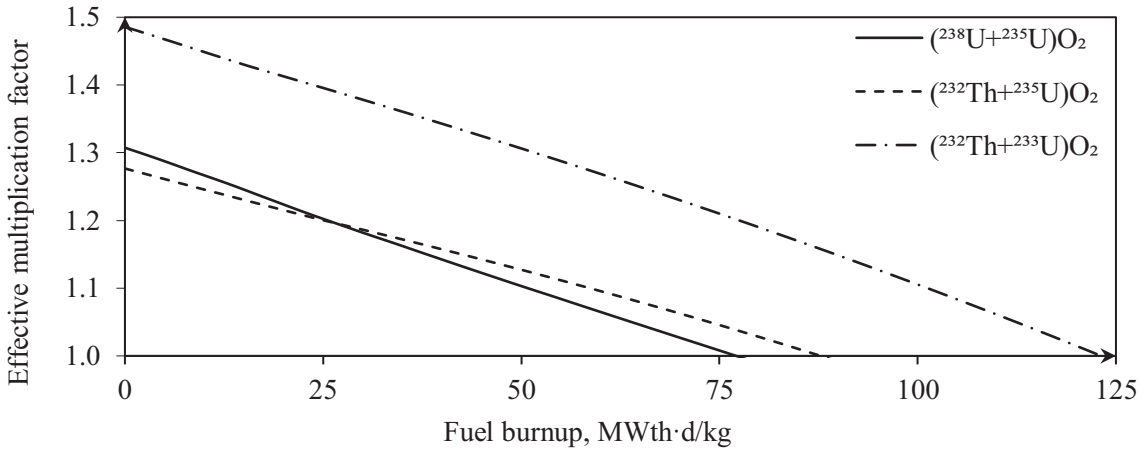

Fig. 4. The dependence of the effective multiplication factor on the fuel burnup.

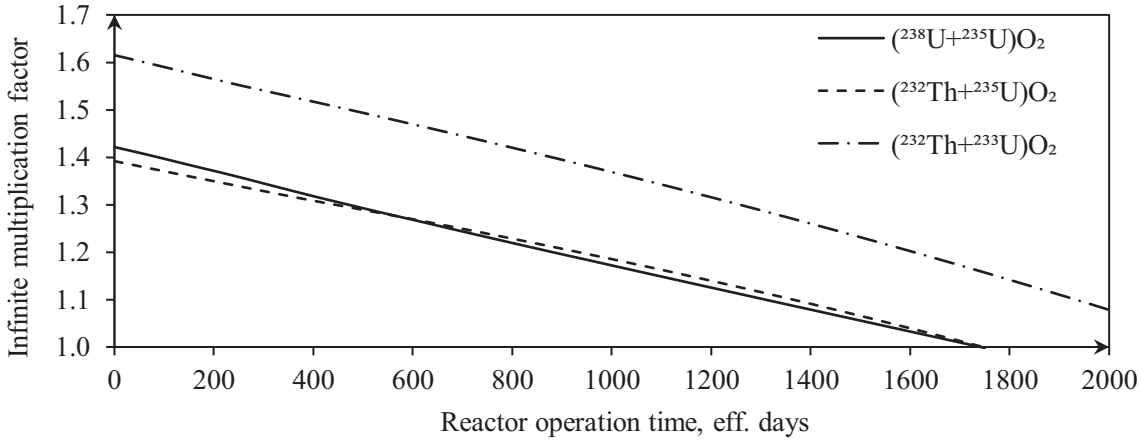

Fig. 5. The dependence of the infinite multiplication factor on the reactor operation time.

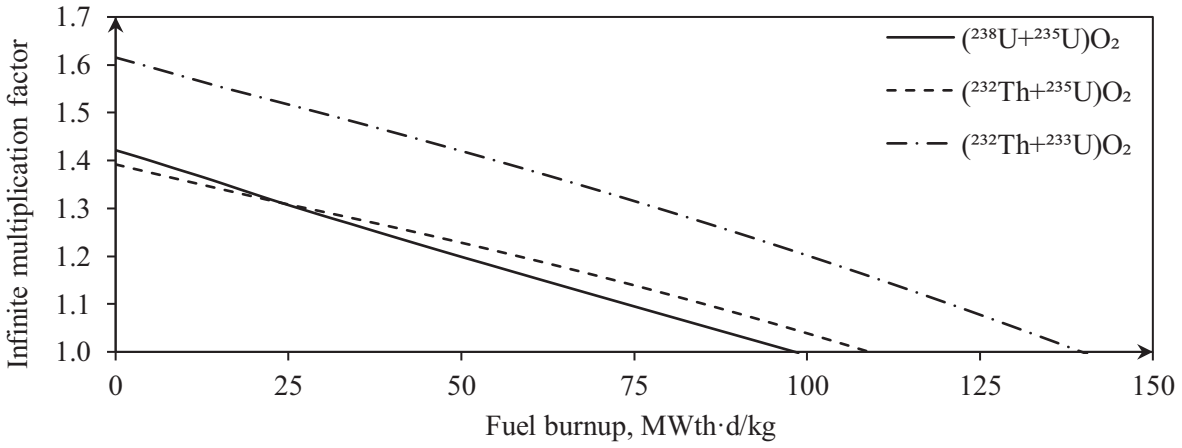

Fig. 6. The dependence of the infinite multiplication factor on the fuel burnup.

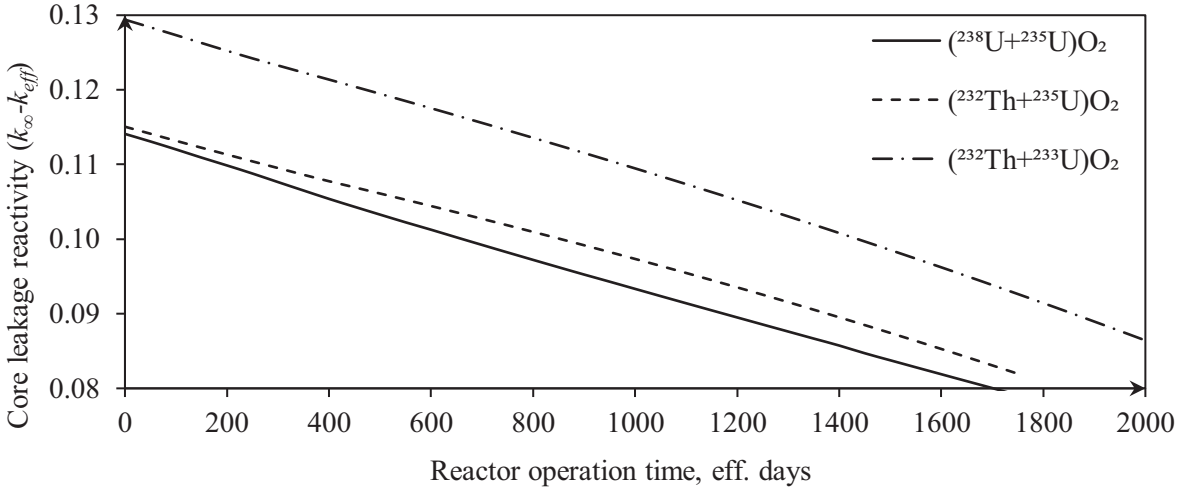

Fig. 7. The dependence of the core leakage reactivity on the reactor operation time.

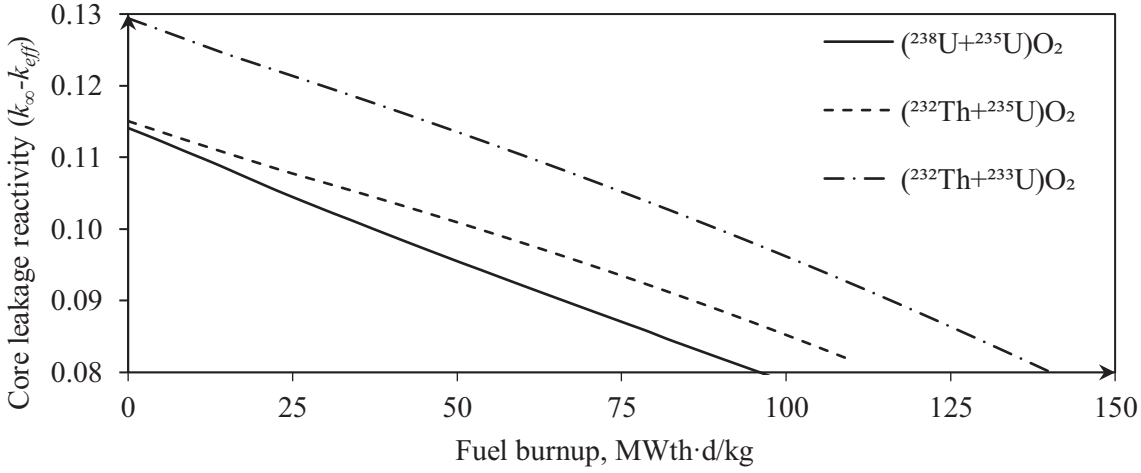

Fig. 8. The dependence of the core leakage reactivity on the reactor operation time.

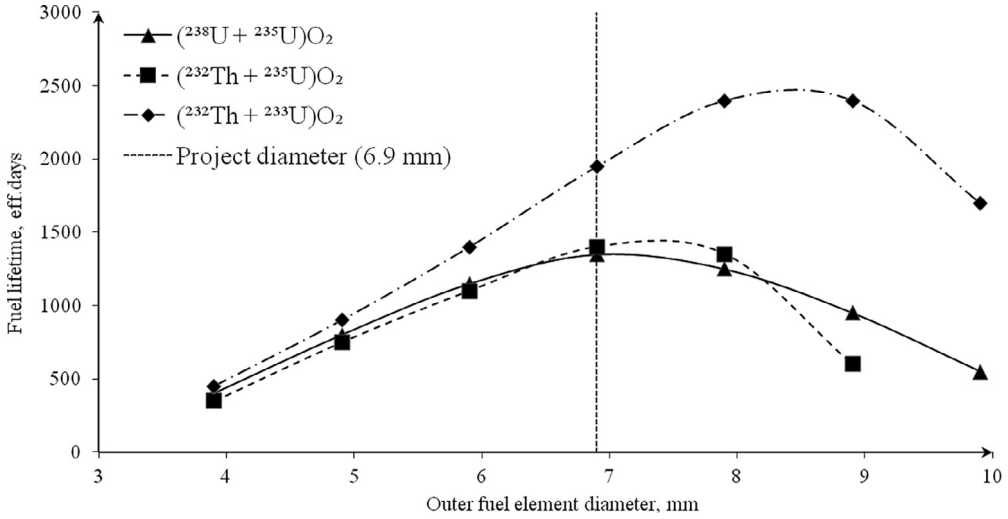

Fig. 9. Dependence of the nuclear fuel lifetime on the fuel element diameter.

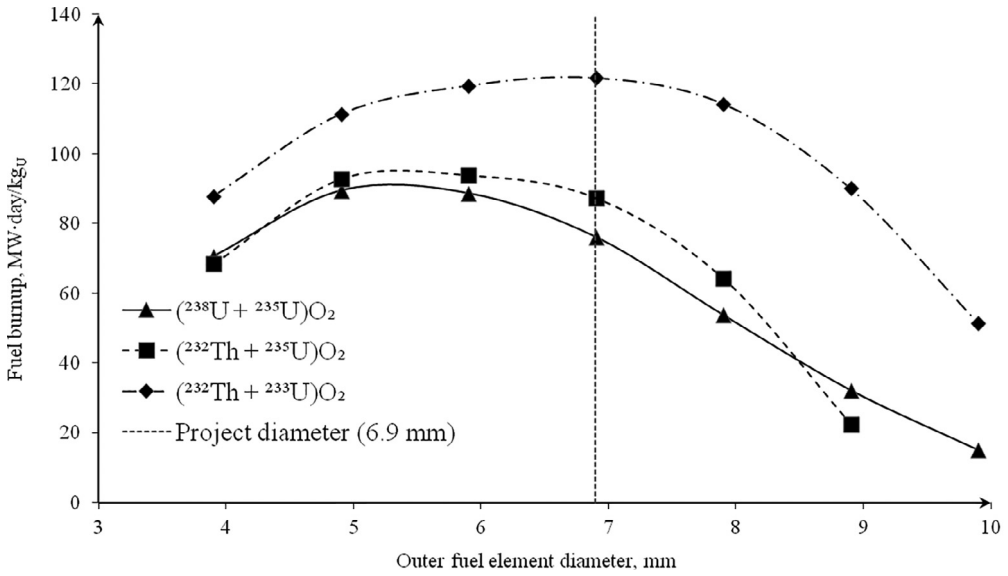

Fig. 10. Dependence of the fuel burnup on the fuel element diameter.

radiative capture process of ^{232}Th (Zakharychev et al., 2019; Du Toit and Naicker, 2018). In addition to that, the values of fissile utilization show that the switch to (^{232}Th + ^{233}U)O_2 leads in the 641 MWth·d/kg_{fiss} value that is two times lower than the value for VVER-1000.

5. Influence of the fuel element diameter on the fuel lifetime

The calculation was carried out for fuel element diameters in the range of 3.9 to 9.9 mm with a step of 1 mm. The design value of the fuel element diameter is 6.9 mm.

Figs. 9-11 describe dependences of the reactivity margin, the fuel lifetime, and the burnup on the fuel element diameter in the three fuel compositions.

The optimal diameter value for (^{238}U + ^{235}U)O_2 is the designed value of 6.9 mm as it provides a 1350 days fuel lifetime. From the point of the highest burnup, the best fuel diameter is 4.9 mm as it provides 89.5 MW·d/kg_U burnup and the fuel lifetime of 800 effective days.

For (^{232}Th + ^{235}U)O_2 composition, the optimal diameter value is also 6.9 mm as it provides 1400 effective days of the fuel lifetime. The fuel diameter of 5.9 mm for this composition provides 93.85 MW·d/kg_{HM}, while the fuel lifetime is 1100 effective days.

For (^{232}Th + ^{233}U)O_2 composition, the optimal diameter is 7.9 mm as it provides 2400 effective days of the fuel lifetime. The design value of 6.9 mm for this composition provides the highest fuel burnup of 121.75 MW·d/kg_{HM} and 1950 effective days of the fuel lifetime.

Therefore, the design diameter value of 6.9 mm is optimal for (^{238}U + ^{235}U)O_2 and (^{232}Th + ^{235}U)O_2 compositions. As concerns (^{232}Th + ^{233}U)O_2, the optimal fuel diameter value is 7.9 mm, since it provides an increase in the fuel lifetime by 77.8% and in the burnup by 50.1% compared to the designed diameter value.

6. Conclusion

In the case of using the (^{238}U + ^{235}U)O_2 and (^{232}Th + ^{235}U)O_2 compositions, there is no need to increase the fuel element

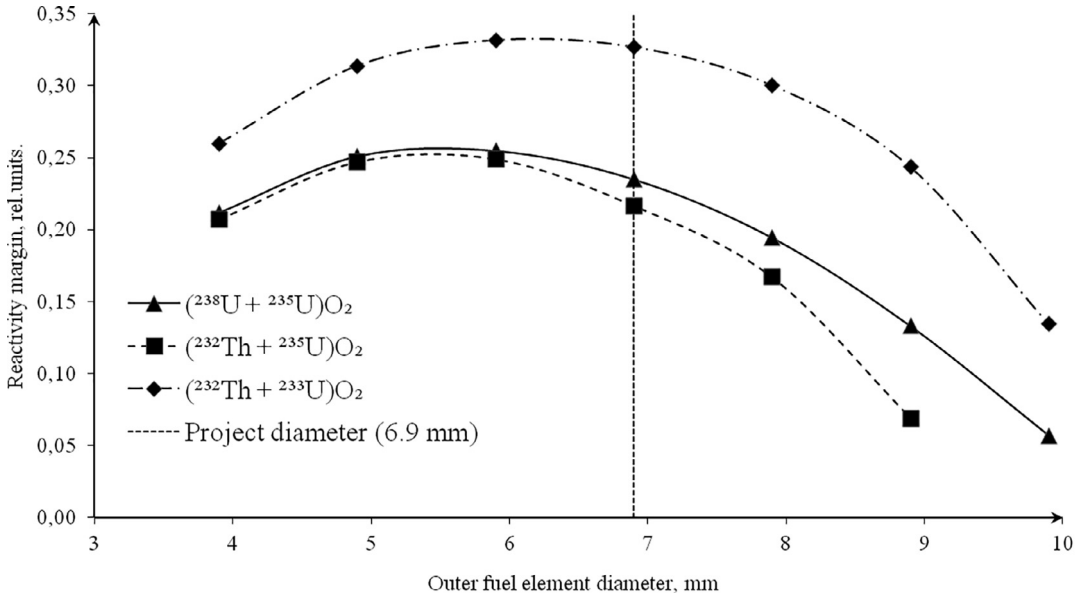

Fig. 11. Dependence of reactivity margin on the fuel element diameter.

diameter, since its designed value provides the optimal fuel lifetime and fuel burnup. The switch from the designed fuel to (^{232}Th + ^{235}U)O_2 provides an increase in the fuel lifetime by 3.7% and fuel burnup 14.7%.

The optimal solution is to use the (^{232}Th + ^{233}U)O_2 composition with a fuel diameter of 7.9 mm. In that case, the fuel lifetime increases by 77.8% and the fuel burnup increases by 50.1% compared to the design values.

7. Future studies

The future studies will be devoted to thermalhydraulic and Monte-Carlo simulations of the KLT-40S and RITM-200 reactors. To justify the switch to thorium-uranium nuclear fuel cycle with thickened fuel element diameter, it is crucial to develop a numeroexperimental approach by means of precision nuclear codes (e.g., WIMS-DB5, MCU, MCNP, Scale, Serpent, and et cetera) to determine key neutronic parameters for the RITM-200 reactor core. Besides, a thickening of the fuel element diameter requires some additional thermohydraulic calculations in order to avoid the departure from nucleate boiling.

If acquired calculation results are acceptable, there can be a switch from such hypothetical fuel types as (^{232}Th + ^{235}U)O_2 and (^{232}Th + ^{233}U)O_2 to a perspective fuel type (Th + Pu)O_2. Plutonium nuclide composition in this fuel type would correlate to the plutonium produced in thermal nuclear reactors (RBMK-1000, VVER-1000, VVER-1200). While conducting the calculations, it is very important to pay special attention to the content of ^{228}Th, ^{232}U, ^{238}Pu in spent fuel, since these nuclides are capable of producing the high radioactivity that leads in radiolysis in spent solutions during the waste fuel recycling.

CRediT authorship contribution statement

S. Beliavskii: Writing – original draft, Visualization, Methodology, Writing – review & editing. **N. Anikin:** Writing – original draft, Formal analysis, Investigation, Data curation. **S. Alhassan:** Writing – review & editing, Validation. **S. Kudeev:** Validation, Visualization. **V. Nesterov:** Conceptualization, Supervision, Project administration.

Declaration of Competing Interest

The authors declare that they have no known competing financial interests or personal relationships that could have appeared to influence the work reported in this paper.

Acknowledgements

This research was supported by the Russian Science Foundation under RSF grant No. 22-29-00385 (https://rscf.ru/en/project/22-29-00385/).

The authors are very grateful to the peer reviewers, whose comments allowed to improve the quality of the paper significantly.

References

Bartolomey, G.G., Bat, G.A., Baybakov, V.D., Alhutov, M.S., 2012. Fundamentals of the Theory and Methods for Design of Nuclear Power Reactors. Energoizdat, Moscow.

Bashmakov, I.A., 2017. Enhancement of power supply efficiency in Northern regions of Russia. Energosberezhenie 3, 58–72.

Bedenko, S.V., Ghal-Eh, N., Lutsik, I.O., Shamanin, I.V., 2019. A fuel for generation IV nuclear energy system: Isotopic composition and radiation characteristics. Appl. Radiat. Isotopes 147, 189–196. https://doi.org/10.1016/j.apradiso.2019.03.005.

Beliavskii, S.V., Nesterov, V.N., Laas, R.A., Godovikh, A.V., Bulakh, O.I., 2020. Effect of fuel nuclide composition on the fuel lifetime of reactor KLT-40S. Nucl. Eng. Des. 360, 110524. https://doi.org/10.1016/j.nucengdes.2020.110524.

Braslavskiy, Y.V., Matuzaev, K.B., Merzlikin, G.Y., Sukrushev, A.V., 2019. Analysis of Economic Efficiency of Long-Term Fuel Cycles Introduction at the NPP with WWER-1000. Energeticheskie ustanovki i tehnologii 5 (1), 7–9.

Du Toit, M.H., Naicker, V.V., 2018. Neutronic design of homogeneous thorium/uranium fuel for 24 month fuel cycles in the European pressurized reactor using MCNP6. Nucl. Eng. Des. 337, 394–405. https://doi.org/10.1016/j.nucengdes.2018.07.023.

Galahom, A.A., Mohsen, M.Y., Amrani, N., 2022. Explore the possible advantages of using thorium-based fuel in a pressurized water reactor (PWR) part 1: neutronic analysis. Nucl. Eng. Technol. 54 (1), 1–10. https://doi.org/10.1016/j.net.2021.07.019.

Ganev, I.H., 1992. Nuclear Reactor Physics. Energoizdat, Moscow.

Golovatskiy, A.V., Nesterov, V.N., Shamanin, I.V., 2010. Organization of the iterative process in the numerical reconstruction of the neutron spectrum in a multiplying system with a graphite moderator. Izvestia Vysshikh Uchebnykh Zavedeniy. Fizika 53, 10–14.

Hernandez, R., Brown, N.R., 2020. Potential fuel cycle performance of floating small modular light water reactors of Russian origin. Ann. Nucl. Energy 144, 107555. https://doi.org/10.1016/j.anucene.2020.107555.

IAEA, 2018. Deployment indicators for small modular reactors. International Atomic Energy Agency https://www-pub.iaea.org/MTCD/Publications/PDF/TE-1854web.pdf.

IAEA, 2020. Nuclear Technology Review. International Atomic Energy Agency. https://www.iaea.org/sites/default/files/gc/gc64-inf2.pdf.

IAEA, 2020. Advances in Small Modular Reactor Technology developments. A Supplement to: IAEA Advanced Reactors Information System (ARIS) 2020 Edition. https://aris.iaea.org/Publications/SMR_Book_2020.pdf.

Karimi, J., Shayesteh, M., Zangian, M., 2021. Core calculations for small modular reactor during burnup cycle. Energy Sources Part A 1–18. https://doi.org/10.1080/15567036.2021.1963883.

Kosheev, V.N., Manturov, G.N., Nikolaev, M.N., Tsiboulya, A.M., 2014. ABBN-RF nuclear data library for calculations of reactor physics and radiation safety. Izvestia Vysshikh Uchebnykh Zavedeniy. Yadernaya Energetika 3, 93–101. https://doi.org/10.26583/npe.2014.3.10.

Kostin, V.I., Samoilov, O.B., Vavilkin, V.N., Panov, Y.K., Kurachenkov, A.V., Bolshukhin, M.A., Pekanov, A.A., 2004. Small floating nuclear power plants with ABV reactors for electric power generation, heat production and sea water desalination. Nuclear technology and societal needs. The 15th annual conference of Indian Nuclear Society.

Krushelnitskii, V.N., 2015. Application field for small modular reactor units. In: Atomnie stantsii maloi moshnosti: novoe napravlenie razvitiia energetiki. Academ-Print, 50-58.

Lebedev, M.P., Shadrin, A.P., 2011. Issues of organic fuel delivery to the North and a role that small modular reactors are playing in Far North. Atomnie stantsii maloi moschnosti: novoe napravlenie razvitiia energetiki, 88–100.

Melnikov, N.N., Gusak, S.A., Naumov, V.A., 2020. Reactor units to supply electricity for arctic regions of Russia: an estimation of nuclear sources priority. Vestnik MSTU 20 (1), 21–30.

Petrunin, V.V., Fadeev, Y.P., Pakhomov, A.N., Veshnyakov, K.B., Polunichev, V.I., Shamanin, I.E., 2019. Conceptual Design of small NPP with RITM-200 Reactor. At. Energ. 125 (6), 365–369. https://doi.org/10.1007/s10512-019-00495-4.

Rose, S.J., Wilson, J.N., Capellan, N., David, S., Guillemin, P., Ivanov, E., Méplan, O., Nuttin, A., Siem, S., 2011. Minimization of actinide waste by multi-recycling of thoriated fuels in the EPR reactor. Ann. Nucl. Energy 38 (11), 2619–2624.

Samoilov, O.B., Alekseev, V.I., Galitskikh, V.Y., Belin, A.V., Zaglyadnov, A.N., Samusenkov, V.V., Ustiantsev, S.G., 2017. Investigation of thermal and epithermal neutron flux distributions in universal nuclear icebreaker fuel assemblies. At. Energ. 121 (6), 389–396. https://doi.org/10.1007/s10512-017-0217-0.

Shamanin, I.V., Bedenko, S.V., Chertkov, Y.B., Gubaydulin, I.M., 2015. Gas-cooled thorium reactor with fuel block of the unified design. Nucl. Energy Technol. 1 (3), 184–190. https://doi.org/10.1016/j.nucet.2016.01.012.

Uguru, E.H., Sani, S.A., Khandaker, M.U., Rabir, M.H., 2020. Investigation on the effect of 238U replacement with 232Th in small modular reactor (SMR) fuel matrix. Prog. Nucl. Energy 118, 103108. https://doi.org/10.1016/j.pnucene.2019.103108.

Zakharychev, A.A., Papotin, Yu.V., Stadnik, D.M., 2019. Cores for small nuclear power plants. In: 11th Conference on Reactor materials engineering. Dimitrovgrad. JSC «GNC-NIIAR», 124-125.

Zmieva, K.A., 2020. Problems of energy supply in the Arctic regions. Russian Arctic 8, 5–14 https://doi.org/10.24411/2658-4255-2020-00001.